Received 11 July 2024; accepted 28 July 2024. Date of publication 2 August 2024; date of current version 13 August 2024.

Digital Object Identifier 10.1109/OJCOMS.2024.3437458

Wideband MIMO THz System Design With MB-OFDM Waveform and Hybrid Beamforming

T. D. DHEERAJLAL (Graduate Student Member, IEEE), AND AMIT KUMAR DUTTA (Member, IEEE)

G. S. Sanyal School of Telecommunications, Indian Institute of Technology Kharagpur, Kharagpur 721302, India

CORRESPONDING AUTHOR: A. K. DUTTA (e-mail: amitdutta@gssst.iitkgp.ac.in)

This work was supported by the MeiTY, Government of India under Grant 13(44)/2020-CCBT.

ABSTRACT Terahertz (THz) band communication, operating in the range of $(0.1-10)\times 10^{12}$ Hz, holds immense potential for fulfilling the ever-increasing demand for ultra-high data rate wireless communication. However, the unfavorable channel characteristics of THz communication pose a significant challenge in realizing this promising technology. In this paper, we present a novel solution to this challenge by proposing a wideband THz hybrid multiple-input multiple-output (MIMO) system design that leverages the ultra-wide bandwidth and the high spectral efficiency of MIMO schemes. We address the frequency-dependent nature of the THz channel by using a filter-bank-based channel model and a multi-bank orthogonal frequency division multiplexing (MB-OFDM) waveform design, which slices the wideband channel into smaller frequency-independent subbands. Specifically, we illustrate two different THz hybrid MIMO structures, one with a single precoder and combiner in the high sampling domain and another with a band-wise precoder design in the low sampling domain. We have adopted sub-optimal methods that alternatively optimize the beamformers. We evaluate the performance of our proposed MIMO schemes using numerical simulations that validate their feasibility and effectiveness in achieving communication in ultra-wideband frequency-dependent THz channels under various parameters and subband width assumptions. The results also indicate that the proposed MB-OFDM waveform design reduces the peak-to-average power ratio (PAPR) of the spatial streams compared to conventional OFDM.

INDEX TERMS THz, filter banks, MB-OFDM, spectral efficiency, wideband MIMO, hybrid beamforming.

I. INTRODUCTION

THE TERAHERTZ (THz) frequency band's ultra-wide bandwidth availability makes it a highly appealing solution to overcome spectrum limitations and meet the ultra-high data rate requirements of future wireless systems [1], [2]. Additionally, the THz band's sub-millimeter wavelength allows for the packing of numerous antennas into small areas, enabling the use of beamforming to overcome significant path loss and ensure adequate signal power reception at THz frequencies [3]. However, to achieve reliable and efficient wireless communication in the THz spectrum, a new digital baseband system design is required that considers the THz-specific channel characteristics, which differ significantly from conventional wireless channels. The THz channel is heavily affected by the frequency-dependent molecular absorption loss [4], [5]. In addition to that, due to the peculiar nature of the THz band, all the other propagation phenomenons like reflection, scattering, and diffraction are also frequency dependent in nature [6], [7], [8], [9] especially as we go higher in the THz frequency ranges. As a result of these highly frequency-dependent nature, the THz channel coefficients cannot be considered constant for the entire bandwidth of interest. Thus, one of the most critical challenges to be addressed in future ultra-wideband THz wireless systems is the frequency-dependent nature of the channel impulse response (CIR). In addition, to realize the ultra-high target data rates, the large bandwidths available in the THz band must be optimally combined with multiple-input multiple-output (MIMO) technologies using large antenna arrays for improved spectral efficiency and thus enabling ultra-high data rates for THz-based future wireless applications. In millimeter wave (mmWave) bands, orthogonal frequency division multiplexing (OFDM) is deployed to address the frequency-selective nature of the channel. However, in THz communication, as the bandwidth of operation is huge, the channel coefficients corresponding

to the frequency-selective MIMO channel in the ultra-wide bandwidth exhibit frequency-dependent characteristics, resulting in distinct frequency-selective behaviors among different subbands within the bandwidth of interest. As a consequence, it becomes crucial to integrate these THz-specific traits into the baseband system design to achieve dependable and efficient ultra-wideband THz communication. Also in the THz band, we need to improve spectral efficiency by keeping the hardware complexity and power consumption at an affordable level. Hybrid precoding improves the performance of MIMO systems with a reduced number of radio frequency (RF) chains by dividing the signal processing between the analog RF and digital baseband domains [10], [11], [12], [13], [14]. There are several works on THz MIMO with hybrid beamforming for wireless communication in the THz band. A hybrid beamforming scheme for multi-carrier systems over frequency selective channels in the THz band was proposed in [15], [16]. Hybrid precoding designs for wideband THz systems considering the beam squint effect are studied in recent works [17], [18], [19], [20], [21], [22]. The authors in [23] discuss the waveform design in joint radar sensing and communication systems in the mmWave wave and low THz bands. A flexible index modulation-aided pilot design for THz communication is discussed in [24].

However, the above works assume the same baseband channel coefficients for the whole bandwidth of interest and do not consider the frequency-dependent nature of the THz channel. In this work, we consider a digital baseband input-output filter bank channel model to incorporate the frequency-dependent nature of the ultra-wideband THz channel and propose a hybrid MIMO system design with a THz-specific waveform that uses a combination of OFDM and filter banks for wideband transmission also known as the multi-bank OFDM (MB-OFDM).

Why MB-OFDM based waveform?: The traditional cyclic-prefix (CP) based OFDM scheme experiences a decrease in spectral efficiency when used in systems with a significantly large bandwidth, primarily due to the inclusion of a substantial CP. Moreover, the high peak-to-average power ratio (PAPR) requirements also make OFDM inefficient when operating in the THz band. Another key bottleneck of the OFDM system is the out-of-band (OoB) emission, which impacts the sideband. However, the MB-OFDM-based system addresses these concerns and offers improvements in this regard. Consequently, the MB-OFDM-based filter bank system emerges as a promising candidate for the waveform in a high-frequency THz system characterized by an ultra-wide bandwidth. The idea of MB-OFDM has been studied and researched over several years and there have been many works based on this concept [25], [26], [27]. An MB-OFDM system was discussed in [28] as an alternative to the offset quadrature amplitude modulation (OQAM) that enhances spectral confinement, i.e., controlling the OoB emission and increases the efficiency with inter-carrier interference presence mainly in the sub-6 GHz. Similar works are discussed in [29], [30], [31]. However, these works concentrate mainly on the spectral efficiency and OoB spectrum leakage in the sub-6 GHz bands and do not consider the ultra-wideband THz aspect with beamforming. Our initial work [32] introduced a novel THz-specific MB-OFDM waveform design tailored for a single-input single-output (SISO) scenario, showcasing its effectiveness in harnessing the available ultra-wide bandwidths within the THz band, while considering the frequency-dependent characteristics of the THz channel. However, to further enhance spectral efficiency while utilizing such extensive bandwidths, it becomes imperative to explore the potential of THz-specific waveforms in a MIMO scenario. However, the possibility of a THz-specific digital waveform based on filter banks and multiple OFDM systems for ultra-wideband transmission with beamforming in a hybrid MIMO scenario is not yet studied to the best of our knowledge making this the first of its kind work that proposes MB-OFDM for wideband THz MIMO communication. Thus, in this work, we address the problem of designing the THz digital back-end to utilize the ultra-wide bandwidth availability in this band effectively so that reliable communication with less number of RF chains and lower-order modulation schemes can be achieved. Specifically, we propose two different hybrid MIMO structures: the first with a single precoder and combiner in the high sampling domain, and the second with a band-wise precoder/combiner design in the low sampling domain, assuming that the channel is known or estimated in both cases. We have employed alternative optimization methods to optimize the beamformers within the proposed MB-OFDM based architectures.

Contributions: Given this background, the contributions of this work are as follows

1) We propose a THz-specific MIMO baseband design based on MB-OFDM waveform. This is the first of its kind work in the context of THz. Our approach incorporates the unique THz channel characteristics into the system modeling along with beamforming. The performance of the proposed MIMO schemes is analyzed using numerical simulations with different parameters and subband widths to validate the feasibility and effectiveness of the proposed schemes. Numerical results show that the proposed scheme of MIMO MB-OFDM reduces the PAPR compared to the conventional OFDM system.
2) We develop a digital baseband input-output filter bank channel model that allows for a bandwise digital back-end design. To address the non-linearity of the THz MIMO channel coefficients due to the ultra-high transmission signal bandwidth, this approach splits the large signal bandwidth into smaller subbands, enabling the channel coefficients to remain invariant over the smaller subbands. As a result, the channel is transformed into parallel MIMO filter banks.

We propose two hybrid beamforming architectures based on the high and low sampling domain of the baseband design.

a) *Hybrid beamforming at high sampling domain:* As the waveform is based on MB-OFDM, the interfacing digital logic with the digial-to-analog/analog-to-digital (DAC/ADC) after the upsampling process works at high speed clock. To leverage this aspect, we propose to design the digital precoder/combiner at this clock speed. This hybrid MIMO scheme in the high-sampling domain, is designed to minimize the mean square error (MSE) of the waveform at the receiver. We can also choose the number of precoder/combiner coefficients to reduce hardware complexity.

b) *Hybrid beamforming at low sampling domain:* We also propose a hybrid MIMO scheme with multiple low-dimensional digital precoders/combiners operating in the low-sampling domain, which processes each subband at a lower clock speed. Digital precoding/combining is performed in the frequency domain for each subband, which operates at a lower clock speed. However, this needs larger number of coefficients to be designed.

Notation: Bold upper and lower case letters denote matrix and vector, respectively. The superscripts $(\cdot)^T$ and $(\cdot)^H$ denote the transpose and conjugate of a matrix, respectively. $\mathbf{E}[\cdot]$ denotes the expectation, while $\mathbf{I}_N$ denotes an $(N \times N)$ identity matrix, Tr(.) represents a trace operation.

II. BACKGROUND: THZ CHANNEL OVERVIEW AND ULTRA WIDEBAND THZ FILTER BANK CHANNEL MODEL

An overview of the THz channel and the wideband filter bank channel model is given below.

A. FREQUENCY DEPENDENT MODEL OF THZ CHANNEL

The frequency response of the wideband THz channel at a particular time t is the superposition of frequency responses of the N_p multi-paths and is given as

$$H(f,t) = \sum_{i=1}^{N_p} H_i(f,t), \tag{1}$$

where the frequency response of the i^{th} multipath is given by

$$H_i(f,t) = |H_i(f,t)|e^{j\angle H_i(f,t)}. \tag{2}$$

In the conventional cellular bands, the magnitude response of the i^{th} path $|H_i(f,t)| = |H_i(t)|$ can be considered independent of frequency because of the narrow signal bandwidth. As the magnitude response $|H_i(f)|$ is flat across the whole bandwidth of interest, we can apply the linear phase criterion on each path, and hence the total frequency response of the channel can be given as

$$H(f,t) = \sum_{i=1}^{N_p} |H_i(t)|e^{-j2\pi f\tau_i(t)}, \tag{3}$$

where τ_i is the propagation delay of the i^{th} multi-path. Therefore, even though the individual attenuation and delays of the multi-paths are assumed to be frequency-independent in conventional narrow bands, the frequency selectivity arises because of the different multipath delays of different paths.

However, in the THz band, the input signal bandwidth spans several GHz, and the magnitude response on each path is frequency-dependent, as it is the product of attenuation due to path loss, molecular absorption loss, and phenomena-dependent loss. The phenomena-dependent loss could be reflection, scattering, or diffraction loss, depending on the nature of the multipath. The magnitude response for the i^{th} path with large bandwidth is given as follows [5]

$$|H_i(f,t)| = \left|H_i^F(f,t)\right| \times \left|H_i^A(f,t)\right| \times \left|H_i^P(f,t)\right|, \tag{4}$$

where $|H_i^F(f,t)^|$ is the attenuation of the i^{th} path due to path loss, $|H_i^A(f,t)|$ is the attenuation on the i^{th} path due to absorption loss and $|H_i^P(f,t)|$ is the phenomena dependent loss on the i^{th} path at time t. Considering a low Doppler in the system design, we ignore the time dependency in (4). Therefore, attenuation due to the path loss is given by [5]

$$\left|H_i^F(f)\right| = \frac{c}{4\pi f d_i}, \tag{5}$$

where c is the speed of light and d_i is the path length of the i^{th} path. The attenuation due to environmental absorption loss is given by [5]

$$\left|H_i^A(f)\right| = e^{-\frac{1}{2}k(f)d_i}, \tag{6}$$

where $k(f)$ is the frequency-dependent absorption coefficient and is given by [4]

$$k(f) = \sum_q \frac{pT_{STP}}{p_0 T} Q^q \sigma^q(f), \tag{7}$$

where p_0 is the standard pressure, T_{STP} is the temperature at standard pressure, p is the pressure, T is the temperature, Q^q is the number of molecules per unit volume of gas q and σ^q is the absorption cross section of gas q. The absorption cross-section depends on the line intensity and the line shape, which are available in the HITRAN database [4].

The phenomena dependent loss $|H_i^P(f)|$ could be due to reflection, scattering, or diffraction depending on the nature of the surface, on which the i^{th} multipath falls. In the case of reflected rays, the phenomena dependent loss depends on the reflection coefficient of the surface which depends on the considered material, shape, and roughness of the surface. Detailed descriptions of the frequency dependency of these propagation phenomena can be found in [5].

As a result of the above-mentioned propagation phenomena in the THz band, the various multi-paths already have a frequency selectivity nature. Therefore, the THz wireless channel will have a frequency selectivity due to the random multipath delays on top of the already existing frequency-dependent nature of the individual multi-paths due to molecular absorption and other frequency-dependent

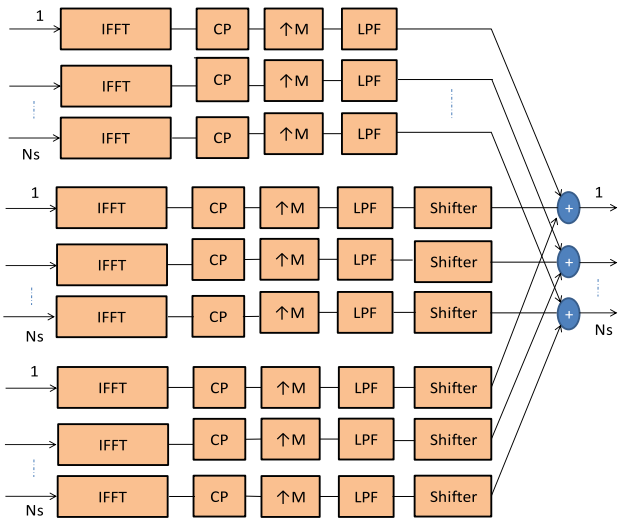

FIGURE 1. Proposed MB-OFDM waveform generation at the transmitter (Excluding beamforming part).

propagation phenomena. Hence, there is a need for an appropriate model that characterizes these effects in a simple and mathematically tractable way.

B. BASEBAND INPUT-OUTPUT FILTER BANK CHANNEL MODEL

In this subsection, we describe the digital input-output filter bank channel model for wideband THz channels. To simplify the THz channel model, the complete wide band is split into M number of smaller subbands. The m^{th} subband will have the frequency response from the i^{th} path $H_i^m(f)$ as an all-pass filter. Assuming a no Doppler scenario, (1) can be rewritten as

$$H(f) = \sum_{m=1}^{M} H^m(f), \tag{8}$$

where $H^m(f)$ is the total channel spectrum at the m^{th} smaller band and can be expressed as

$$H^m(f) = \sum_{i=1}^{N_p} H_i^m(f). \tag{9}$$

Now, (9) can be realized in the digital domain using finite impulse response (FIR) filter with the coefficients as [33]

$$\mathbf{h}^m = \left[h_0^m h_1^m \dots h_{L-1}^m\right], \tag{10}$$

where h_i^m represents the i^{th} discrete channel coefficient for the m^{th} band. Therefore, using (9) and (10), we can approximate the entire wideband THz channel as a parallel FIR filter bank where the filter coefficients remain approximately frequency-invariant across the smaller subbands.

III. MB-OFDM BASED WAVEFORM DESIGN FOR THz MIMO BASED ON FILTER BANK CHANNEL MODEL

In this section, we describe the proposed THz-specific MB-OFDM waveform design for wideband MIMO communications. We initially present the proposed waveform design for THz MIMO utilizing MB-OFDM without beamforming for the ease of data model description. Subsequently, we describe the two proposed beamforming parts separately. The transmitted waveform for THz MIMO is designed to contain multiple independent narrow-band MIMO data, which are separated in the spectral domain from each other. The various stages of the proposed waveform design are as follows.

A. TRANSMITTER DESIGN WITH MB-OFDM FOR MIMO

In this subsection, we describe the various stages of the baseband transmitter design of the proposed MB-OFDM based MIMO system.

1) STAGE-1: MULTIPLE MIMO OFDM SYSTEMS

The total transmission bandwidth B_t is subdivided into M number of smaller subbands. Each subband is further subdivided to have $K = \lfloor \frac{B_t}{M\Delta f} \rfloor$ number of subcarriers where Δf is the subcarrier spacing. Zero padding is carried out at the beginning and at the end of each subband to avoid interference between neighboring subbands. We denote K_e as the effective number of non-zero subcarriers in each subband and assume that $N_z = (K - K_e)$ number of zeros are added at each subband. We have N_s number of spatial streams corresponding to each of the M subbands. The frequency domain symbol vector corresponding to the i^{th} spatial stream in the m^{th} subband, including the zero padding, is denoted as $\mathbf{b}_i^m \in \mathbf{C}^{K\times 1}, i = 1, 2, \dots, .N_s$, where K is the total number of subcarriers in a subband. The frequency domain MIMO data vector corresponding to the m^{th} subband at the k^{th} subcarrier is denoted as $\mathbf{b}^m[k] \in \mathbf{C}^{N_s\times 1}, k = 1, 2, \dots, .K$. Now, K-point inverse fast Fourier transform (IFFT) is carried out on each stream $\mathbf{b}_i^m$ corresponding to the individual subbands. By arranging the frequency domain vectors in matrix form as $\mathbf{B} \in \mathbf{C}^{K\times N_s}$, we can represent the time domain data corresponding to the m^{th} band as $\mathbf{D}^m \in \mathbf{C}^{K\times N_s} = \mathbf{F}^H\mathbf{B}^m$, where $\mathbf{F}^H$ is the $K \times K$ IFFT matrix. The resulting time domain data for the i^{th} stream in the m^{th} subband is denoted as $\mathbf{d}_i^m \in \mathbf{C}^{(K+L_c)\times 1}, i = 1, 2, \dots, N_s$ after the CP addition, where L_c is the length of the CP. Thus, after stage 1, we have M number of time domain MIMO sequences of size $N_s \times (K+L_c)$ corresponding to the frequency domain MIMO symbol data of size $N_s \times K$ of the M subbands.

2) STAGE-2: UPSAMPLING AND INTERPOLATION FILTERING

In the next stage, the $\mathbf{d}_i^m$ sequence is upsampled by a factor M to obtain the new sequence $\mathbf{d_1}_i^m \in \mathbf{C}^{M(K+L_c)\times 1}, i = 1, 2, \dots, N_s$. Thus, the upsampled sequence in the m^{th} subband for the i^{th} stream at the n^{th} discrete time is given as

$$d_1{}_i^m[n] = d_i^m[n/M], \text{ when } n \text{ is divisible by } M$$
$$0, \text{otherwise.} \tag{11}$$

Therefore in the Z-domain, we have

$$D_{1_i}^{m}(z) = D_i^m(z)z^{-M}, \tag{12}$$

where $D_i^m(z)$ is the z-transform of the sequence $d_i^m[n]$ and is defined as

$$D_i^m(z) = \frac{1}{\sqrt{N}} \sum_{l=0}^{N+L_c-1} \left[\sum_{n=0}^{N-1} e^{-j\omega ln/N} d_i^m[n] \right] z^{-l} \tag{13}$$

After the upsampling, a low pass filtering (LPF) operation is carried out using an LPF with transfer function $G_1(z)$ having a normalized cut-off frequency of π/M on each of the spatial streams in all the subbands. The resulting filtered sequence in the m^{th} band is denoted as $d_{2_i}^m[n]$ with

$$D_{2_i}^m(z) = D_{1_i}^m(z)G_1(z), i = 1, 2, \ldots, N_s, \tag{14}$$

where $D_{2_i}^m(z)$ is the z-transform of the i^{th} sequence after filtering and $G_1(z)$ is the transfer function of the LPF having a cut-off frequency of π/M. Thus, the upsampling and interpolation filtering in the second stage compress and band-limit the spectrum of all the individual time-domain MIMO sequences to π/M.

3) STAGE-3: ORTHOGONAL SPECTRUM SHIFTING AND COMBINING

In the next stage, a band-shifting operation by multiples of π/M is performed on each of the individual band-limited time domain MIMO sequences such that each one of them is orthogonal in the spectral domain. The time domain sequence for the i^{th} spatial stream corresponding to the shifted spectrum of the m^{th} sub-band is denoted as $d_{3_i}^m[n]$ and its spectrum is given by

$$D_{3_i}^m(\omega) = D_{2_i}^m\left(\omega - \frac{(m-1)\pi}{M}\right), \text{for } i = 1, 2, \ldots, N_s. \tag{15}$$

The final step is the addition of all the information-carrying time domain sequences having an orthogonal spectrum to generate the single digital waveform sequence corresponding to each of the streams. Therefore, the final waveform sequence for the i^{th} stream in time domain, $d_i^t[n]$ is given by

$$d_i^t[n] = \sum_{m=1}^{M} d_{3_i}^m[n], i = 1, 2, \ldots, N_s \tag{16}$$

Thus, each spatial stream in the final MIMO waveform contains information corresponding to the M different subbands and such a waveform design allows us to transmit multiple independent narrow-band MIMO data streams simultaneously by utilizing the wide transmission bandwidth available in the THz spectrum. Furthermore, the band-splitting nature coupled with filtering post-upsampling within each subband leads to a significantly reduced PAPR for the proposed waveform, in contrast to the conventional CP-based OFDM. This characteristic renders the proposed waveform a more suitable choice, particularly due to the prevalent non-linearity issues of power amplifiers in THz communication systems.

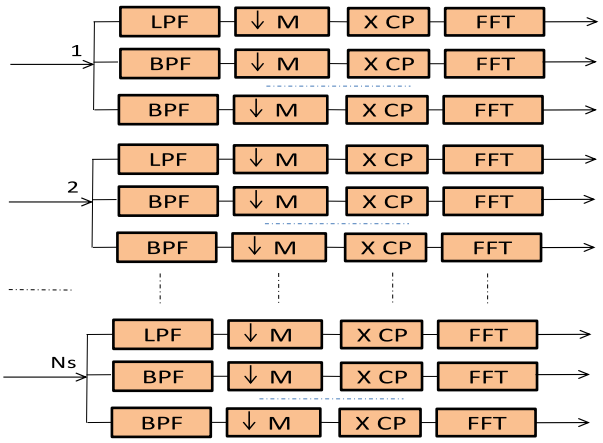

FIGURE 2. MB-OFDM based receiver design (Excluding beamforming part).

B. RECEIVER DESIGN BASED ON THE PROPOSED WAVEFORM

In this subsection, we describe the various stages of the baseband receiver design of the proposed MB-OFDM based MIMO system.

At the receiver, the received data occupying the wide band in the high sampling domain is subjected to a series of reverse operations. The various stages of the receiver design based on the proposed waveform design are as follows

1) BAND PASS FILTERING

The first stage involves band pass filtering of the received data to separate the different MIMO received sequences corresponding to the different individual narrow band MIMO data streams. This can be implemented by first shifting the desired subband to the baseband area, followed by LPF filtering. The shifter at the transmitter and the shifter at the receiver are the same, with only the reverse direction of the band shifting with respect to each other. The frequency spectrum of the output sequence for the i^{th} stream in the m^{th} subband $y_i^m[n]$ will be as follows

$$Y_i^m(\omega) = Y_i\left(\omega + \frac{m\pi}{M}\right)G_2(\omega), \text{ for } i = 1, 2, \ldots, N_s \tag{17}$$

where $Y_i(\omega)$ and $G_2(\omega)$ are the frequency spectrum of the received sequence $y_i[n]$ and LPF having cutoff at π/M respectively. This will result in M number of received time domain MIMO sequences band-limited to π/M corresponding to the individual subbands.

2) DOWN SAMPLING

The next step is the down-sampling of the time domain sequence $y_i^m[n]$ by the factor M. Let us define $Y_{d_i}^m(\omega)$ as the spectrum of the down-sampled sequence corresponding to the i^{th} stream for the m^{th} subband. This is defined as follows

$$Y_{d_i}^m(\omega) = \frac{1}{M} \sum_{k=0}^{M-1} Y_i^m e^{j(\omega - 2\pi k)/M}. \tag{18}$$

Let us assume that the time domain sequence corresponding to the i^{th} stream of (18) after CP discarding is $y_{d_i}^m[n]$ for $n = 0, 1, \ldots, K-1$. Therefore, after performing the K-point FFT operation on each of the time domain sequence vectors in each subband, the discrete frequency domain MIMO data model corresponding to the m^{th} subband becomes

$$\mathbf{y}_d^m[k] = \mathbf{H}_d^m[k]\mathbf{b}^m[k] + \mathbf{w}^m[k], \text{ for } k = 1, 2, \ldots, K \quad (19)$$

where $\mathbf{y}_d^m[k]$ is the $N_s \times 1$ received frequency domain data vector across the k^{th} subcarrier in the m^{th} subband, $\mathbf{H}_d^m[k]$ is the effective frequency domain MIMO channel matrix of subcarrier k in the m^{th} subband, $\mathbf{b}^m[k]$ is the $N_s \times 1$ frequency domain data vector corresponding to the k^{th} subcarrier in the m^{th} subband and $\mathbf{w}^m[k]$ is the corresponding noise vector. The frequency domain channel corresponding to each subband is the Fourier transform of the corresponding effective downsampled frequency-selective MIMO channels. Thus, with such a waveform design, the ultra-wideband THz MIMO system is effectively converted into multiple MIMO systems corresponding to different subbands, which gives us the flexibility of bandwise estimation/detection and compensation.

Remarks on complexity: Here, we analyze the structural complexity of the proposed THz MIMO MB-OFDM system. The K-point IFFT utilizing a radix-2 structure necessitates $(K^2 - K)$ additions and $(K^2/2 + K/2)$ multiplications. Following upsampling, the front-end filters with a finite length of L_1 taps require $(L_1 - 1)$ additions and L_1 multiplications per spatial stream. Consequently, the total complexity in either the transmitter or receiver, considering M subbands and N_s spatial streams, is expressed as $MN_s[\frac{3K^2}{2} - \frac{K}{2} + 2L_1 - 1]$.

IV. PROPOSED MB-OFDM BASED TH$_Z$ HYBRID BEAMFORMING IN MIMO SYSTEMS

In this section, we describe the proposed hybrid beamforming architectures for MB-OFDM based THz MIMO communications. We propose two hybrid beamforming architectures, differentiated by their operation in the high and low sampling domains of the baseband design. To validate the feasibility and effectiveness of our proposed schemes, we employ a simplified optimization process for the THz-specific MB-OFDM-based hybrid MIMO architectures. In this process, we first fix the RF beamformers, which are uniform across all subbands, using existing techniques. Subsequently, we optimize the baseband precoders by accounting for the frequency-dependent variations inherent to the THz channel. This approach leverages alternative optimization techniques to derive the beamformers within the context of the proposed MB-OFDM-based framework.

A. SYSTEM MODEL

We consider an ultra-wideband indoor THz hybrid MIMO wireless system with a transmitter having N_t number of transmit antennas and a receiver with N_r number of receive antennas. The transmitter and receiver have N_{RF} number of RF chains. The analog beamforming at the transmitter and the analog combining at the receiver are assumed to be implemented using digitally controlled THz phase shifters. We consider a fully connected architecture for the RF precoder and RF combiner, even though the schemes can be applied to partially connected architectures as well. We assume that the transmitter is equipped with a uniform linear array (ULA) having N_t antennas, each of which is connected to a THz phase shifter. The transmitter employs the proposed THz-specific filter-bank-based waveform to transmit the data. We propose two beamforming schemes, one in the high sampling domain and the other one in the low sampling domain of the baseband design. Given that the primary objective of this work is to test and evaluate the effectiveness of the proposed schemes in mitigating the frequency-dependent characteristics of the THz channel, we adopt the assumption of an ideal and complete channel state information (CSI) scenario. Nonetheless, by making this assumption, we create opportunities for future exploration into scenarios involving imperfect CSI and other impairments, such as beam squint, thereby paving the way for further research on the proposed schemes.

B. THZ HYBRID MIMO SYSTEM WITH BEAMFORMING IN THE HIGH SAMPLING DOMAIN

In this subsection, we describe the proposed hybrid beamforming architecture with beamforming in the high sampling domain. Given that the waveform is based on MB-OFDM, the digital logic interfacing with the DAC/ADC operates at a high-speed clock after the upsampling process. To take advantage of this, we propose designing the digital precoder and combiner to function at this high clock speed. This hybrid MIMO scheme, working in the high-sampling domain, aims to minimize the MSE of the waveform at the receiver. Additionally, we can adjust the number of precoder and combiner coefficients to decrease hardware complexity.

In this scheme, both the baseband precoding and RF beamforming are performed in the high sampling domain, and we assume that the CSI is completely known at the transmitter. In this scheme, hybrid beamforming is designed to achieve a MIMO transmission over a frequency-dependent MIMO channel. Therefore, the objective of the hybrid beamforming design in the high sampling domain is to design the hybrid precoders at the transmitter and the hybrid combiners at the receiver such that the MSE of the waveform data at the receiver is minimized. The transmitter architecture of the proposed scheme is shown in Fig. 3.

Digital beamforming is used to map the waveform streams into the RF chains. We consider baseband data from (16) at the n^{th} time as $\mathbf{d}^t[n] = [d_1^t[n], d_2^t[n], \ldots, d_{N_s}^t[n]]^T$. These are precoded using the baseband precoder $\mathbf{F}_{BB} \in \mathbf{C}^{N_{RF} \times N_s}$ to form the precoded data as $\mathbf{x}^p[n] = \mathbf{F}_{BB}\mathbf{d}^t[n] \in \mathbf{C}^{N_{RF} \times 1}$.

Our objective is to design an optimal precoder and optimal combiner such that the MSE of the actual transmitted MIMO waveform data and the corresponding received data are minimized. The transmitter uses the analog beamforming

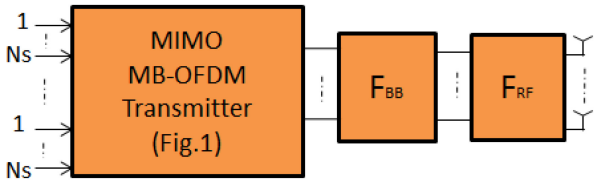

FIGURE 3. Transmitter architecture for THz hybrid MIMO system with single precoder/combiner in the high sampling domain.

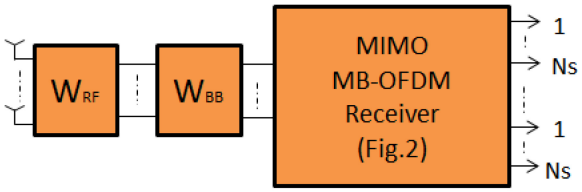

FIGURE 4. Receiver architecture for THz hybrid MIMO system with single precoder/combiner in the high sampling domain.

matrix $\mathbf{F}_{RF} \in \mathbf{C}^{N_t \times N_{RF}}$ to transmit the precoded input waveform $\mathbf{x}^p$ and the received signal is combined using the analog combiner matrix $\mathbf{W}_{RF} \in \mathbf{C}^{N_r \times N_{RF}}$. We maintain that $|\mathbf{F}_{RF}(i,j)| = 1, |\mathbf{W}_{RF}(i,j)| = 1, \forall (i,j)$. Assuming a single tap channel, the baseband received vector $\mathbf{y}[n] \in \mathbf{C}^{N_{RF} \times 1}$ at the n^{th} discrete time after the analog combiner can be written as

$$\mathbf{y}[n] = \left[\mathbf{W}_{RF}^H \mathbf{H} \mathbf{F}_{RF}\right] \mathbf{x}^p[n] + \mathbf{W}_{RF}^H \mathbf{w}[n], \tag{20}$$

where $\mathbf{H}$ is the $N_r \times N_t$ wideband THz channel matrix with high sampling rate and $\mathbf{w}[n]$ is the additive white Gaussian noise (AWGN) vector. As the THz channel can be assumed to be more sparser than a mmWave channel, we use the geometric channel model with a very small number of dominant paths to characterize the THz channel. Since the path gain is highly frequency dependent, we approximate the path gain to be frequency invariant over the smaller subbands. Therefore, the channel can be expressed as

$$\mathbf{H} = \sum_{m=1}^{M} \sum_{l=1}^{L} \alpha_l^m \mathbf{a_R}\left(\theta_l^r, \phi_l^r\right) \mathbf{a_T}^H\left(\theta_l^t, \phi_l^t\right), \tag{21}$$

where L is the number of dominant paths, $\theta_l^t, \theta_l^r \in [0, \pi]$ and $\phi_l^t, \phi_l^r \in [0, 2\pi]$ are the associated elevation angle and azimuth angles for both angles of departure (AoD) and angle of arrival (AoA), M is the number of subbands and α_l^m is the path gain of the l^{th} path in the m^{th} subband. Similarly, $\mathbf{a_R}(\theta_l^r, \phi_l^r) \in \mathbf{C}^{N_r \times 1}$ and $\mathbf{a_T}(\theta_l^t, \phi_l^t) \in \mathbf{C}^{N_t \times 1}$ are the array response vectors associated with the l^{th} path in the receiver and transmitter, respectively. In the case of ULAs, the array response vectors at the transmitter and receiver can be written as

$$\mathbf{a_T}\left(\theta_l^t\right) = \frac{1}{\sqrt{N_t}}\left[1, e^{j\frac{2\pi}{\lambda} d \sin\theta_l^t}, \ldots, e^{j(N_t-1)\frac{2\pi}{\lambda} d \sin\theta_l^t}\right]^T, \tag{22}$$

$$\mathbf{a_R}\left(\theta_l^r\right) = \frac{1}{\sqrt{N_r}}\left[1, e^{j\frac{2\pi}{\lambda} d \sin\theta_l^r}, \ldots, e^{j(N_r-1)\frac{2\pi}{\lambda} d \sin\theta_l^r}\right]^T. \tag{23}$$

The ultra-wideband THz channel matrix is written as follows

$$\mathbf{H} = \sum_{m=1}^{M} \mathbf{H}^m e^{j(m-1)\omega_0 n}, \tag{24}$$

where $\mathbf{H}^m$ is the equivalent low pass channel matrix corresponding to the m^{th} subband and ω_0 is the subband width. It is assumed that the channel matrices $\mathbf{H}^1, \mathbf{H}^2, \ldots, \mathbf{H}^M$ are perfectly known at the transmitter. Therefore, the received data can be written as

$$\mathbf{y}[n] = \mathbf{W}_{RF}^H \left[\mathbf{H}^1 \quad \mathbf{H}^2 e^{j\omega_0 n} \quad \cdots \quad \mathbf{H}^M e^{j(M-1)\omega_0 n}\right] \times \begin{bmatrix} \mathbf{I}_{Nt} \\ \mathbf{I}_{Nt} \\ \vdots \\ \mathbf{I}_{Nt} \end{bmatrix} \mathbf{F}_{RF} \mathbf{x}^p[n] + \mathbf{W}_{RF}^H \mathbf{w}[n] \tag{25}$$

Now, ignoring the discrete-time notion for notational simplicity the data model can be written as

$$\mathbf{y} = \mathbf{W}_{RF}^H \mathbf{H}_E \mathbf{F}_{RF} \mathbf{x}^p + \mathbf{W}_{RF}^H \mathbf{w}, \tag{26}$$

where $\mathbf{H}_E \triangleq \sum_{m=1}^{M} \mathbf{H}^m e^{j(m-1)\omega_0 n} \in \mathbf{C}^{N_r \times N_t}$ is the effective channel matrix. Now, the received data vector $\mathbf{y}$ is processed using the optimal baseband combiner $\mathbf{W}_{BB} \in \mathbf{C}^{N_s \times N_{RF}}$ to recover the original waveform stream. Thus, the final recovered data can be written as follows

$$\hat{\mathbf{d}}^t = \mathbf{W}_{BB} \mathbf{W}_{RF}^H \mathbf{H}_E \mathbf{F}_{RF} \mathbf{F}_{BB} \mathbf{d}^t + \mathbf{W}_{BB} \mathbf{W}_{RF}^H \mathbf{w}. \tag{27}$$

The objective of the optimization problem is to design the hybrid analog and digital precoders at the transmitter and receiver to minimize the MSE of the recovered stream by minimizing the trace of the error covariance matrix given by

$$\mathbf{MSE} = E\left\{\left(\hat{\mathbf{d}}^t - \mathbf{d}^t\right)\left(\hat{\mathbf{d}}^t - \mathbf{d}^t\right)^H\right\}. \tag{28}$$

To reduce the complexity and to illustrate the feasibility of the proposed schemes, we set the analog precoder $\mathbf{F}_{RF}$ and the analog combiner $\mathbf{W}_{RF}$ as the array response vectors corresponding to the actual angles of propagation paths at the transmitter and receiver [10], [34]. Thus

$$\mathbf{F}_{RF} = \left[\mathbf{a_T}\left(\theta_1^t\right) \quad \mathbf{a_T}\left(\theta_2^t\right) \quad \cdots \quad \mathbf{a_T}\left(\theta_L^t\right)\right] \tag{29}$$

$$\mathbf{W}_{RF} = \left[\mathbf{a_R}\left(\theta_1^r\right) \quad \mathbf{a_R}\left(\theta_2^r\right) \quad \cdots \quad \mathbf{a_R}\left(\theta_L^r\right)\right] \tag{30}$$

Then, we design the optimal baseband precoder and combiner, which minimizes the MSE at the receiver. Therefore, after the analog beamforming and combining, the final data model can be written as

$$\hat{\mathbf{d}}^t = \mathbf{W}_{BB} \mathbf{H}_F \mathbf{F}_{BB} \mathbf{d}^t + \mathbf{W}_{BB} \mathbf{n}, \tag{31}$$

where $\mathbf{H}_F = \mathbf{W}_{RF}^H \mathbf{H}_E \mathbf{F}_{RF}$ is the final effective channel after the analog beamforming and combining and $\mathbf{n} = \mathbf{W}_{RF}^H \mathbf{w}$ is the effective noise after the analog combining. Now, substituting (31) into (28), we can express the MSE as follows

$$MSE = \mathrm{Tr}\Big[(\mathbf{W}_{BB}\mathbf{H}_F\mathbf{F}_{BB} - \mathbf{I})\mathbf{R}_{dd}(\mathbf{W}_{BB}\mathbf{H}_F\mathbf{F}_{BB} - \mathbf{I})^H\Big] + \mathrm{Tr}\Big[\mathbf{W}_{BB}\mathbf{R}_{nn}\mathbf{W}_{BB}^H\Big], \quad (32)$$

where $\mathbf{R}_{dd}$ is the covariance matrix of the waveform and $\mathbf{R}_{nn}$ is the noise covariance matrix. Now we have to design the optimal baseband precoder $\mathbf{F}_{BB}$ and the baseband combiner $\mathbf{W}_{BB}$ such that the overall MSE is minimized. Thus, the optimization problem can be written as

$$\underset{\mathbf{F}_{BB},\mathbf{W}_{BB}}{\arg \min} MSE \quad \text{s.t. } \mathrm{Tr}\Big(\mathbf{F}_{BB}\mathbf{R}_{dd}\mathbf{F}_{BB}^H\Big) \le P_{tot}, \quad (33)$$

where P_{tot} is the total transmitted power. Applying the Lagrange method, we can rewrite the modified objective function as follows

$$MSE = \mathrm{Tr}\Big((\mathbf{W}_{BB}\mathbf{H}_F\mathbf{F}_{BB} - \mathbf{I})\mathbf{R}_{dd}(\mathbf{W}_{BB}\mathbf{H}_F\mathbf{F}_{BB} - \mathbf{I})^H\Big) + \mathrm{Tr}\Big(\mathbf{W}_{BB}\mathbf{R}_{nn}\mathbf{W}_{BB}^H\Big) + \mu\Big(\mathrm{Tr}\Big(\mathbf{F}_{BB}\mathbf{R}_{dd}\mathbf{F}_{BB}^H\Big) - P_{tot}\Big), \quad (34)$$

where μ is the Lagrange coefficient. By differentiating the gradient with respect to $\mathbf{W}_{BB}$ and equating it to zero, we obtain the solution of $\mathbf{W}_{BB}$ as

$$\mathbf{W}_{BB} = \mathbf{R}_{dd}\mathbf{F}_{BB}^H\mathbf{H}_F^H\Big(\mathbf{R}_{nn} + \mathbf{H}_F\mathbf{F}_{BB}\mathbf{R}_{dd}\mathbf{F}_{BB}^H\mathbf{H}_F^H\Big)^{-1}. \quad (35)$$

Similarly, by solving $\mathbf{F}_{BB}$, we obtain it as follows

$$\mathbf{F}_{BB} = \Big(\mathbf{H}_F^H\mathbf{W}_{BB}^H\mathbf{W}_{BB}\mathbf{H}_F + \mu\mathbf{I}\Big)^{-1}\mathbf{H}_F^H\mathbf{W}_{BB}^H. \quad (36)$$

Since solving equations (35) and (36) for $\mathbf{W}_{BB}$ and $\mathbf{F}_{BB}$ with the constraint $\mathrm{Tr}(\mathbf{F}_{BB}\mathbf{R}_{dd}\mathbf{F}_{BB}^H) \le P_{tot}$ is difficult, we simplify the objective function in (34) by diagonalizing the symmetric matrices involving $\mathbf{R}_{nn}$, $\mathbf{H}_F$ and $\mathbf{R}_{dd}$ and we focus on $\mathbf{W}_{BB}$ and $\mathbf{F}_{BB}$ that can be decomposed as

$$\mathbf{F}_{BB} = \mathbf{V}\mathbf{\Phi}\mathbf{U}^H, \mathbf{W}_{BB} = \mathbf{U}\mathbf{\Gamma}\mathbf{\Lambda}^{-1}\mathbf{V}^H\mathbf{H}_F^H\mathbf{R}_{nn}^{-1}, \quad (37)$$

where $\mathbf{U}$,$\mathbf{V}$ are the unitary matrices corresponding to the eigen decomposition of $\mathbf{R}_{dd}$ and $\mathbf{H}_F^H\mathbf{R}_{nn}^{-1}\mathbf{H}_F$, respectively and $\mathbf{\Phi}$, $\mathbf{\Gamma}$ are appropriately defined matrices. The involved eigen decomposition are

$$\mathbf{R}_{dd} = \mathbf{U}\mathbf{\Delta}\mathbf{U}^H, \quad (38)$$

$$\mathbf{H}_F^H\mathbf{R}_{nn}^{-1}\mathbf{H}_F = \mathbf{V}\mathbf{\Lambda}\mathbf{V}^H, \quad (39)$$

where $\mathbf{\Delta}$ and $\mathbf{\Lambda}$ are the diagonal matrices containing the eigenvalues corresponding to the respective eigen decomposition. Now by substituting using (37), we can write the objective function (34) as

$$MSE = \mathrm{Tr}\Big(\mathbf{\Gamma}\mathbf{\Lambda}^{-1}\mathbf{\Gamma}^H\Big) + \mathrm{Tr}\Big((\mathbf{\Gamma}\mathbf{\Phi} - \mathbf{I})\mathbf{\Delta}(\mathbf{\Gamma}\mathbf{\Phi} - \mathbf{I})^H\Big) + \mu\Big(\mathrm{Tr}\Big(\mathbf{\Phi}\mathbf{\Delta}\mathbf{\Phi}^H\Big) - P_{tot}\Big). \quad (40)$$

Equating to zero the derivatives of (40) with respect to $\mathbf{\Phi}$ and $\mathbf{\Gamma}$ we obtain

$$\mathbf{\Phi} = \Big(\mathbf{\Gamma}^H\mathbf{\Gamma} + \mu\mathbf{I}\Big)^{-1}\mathbf{\Gamma}^H, \quad (41)$$

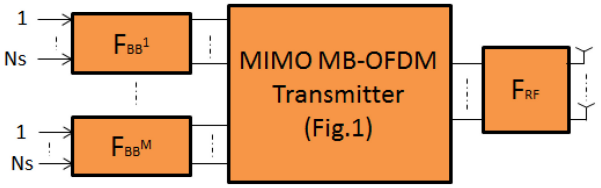

FIGURE 5. Transmitter architecture for ultra-wideband THz MIMO with band-wise precoders/combiners.

and

$$\mathbf{\Gamma} = \mathbf{\Delta}\mathbf{\Phi}^H\Big(\mathbf{\Lambda}^{-1} + \mathbf{\Phi}\mathbf{\Delta}\mathbf{\Phi}^H\Big)^{-1}, \quad (42)$$

respectively. Following [35] and using (41), (42), the objective function can be further simplified to obtain the diagonal matrix $\mathbf{\Phi}$ with the $(i,i)^{th}$ entry as follows

$$|\phi_{i,i}|^2 = \frac{P_{tot} + \mathrm{Tr}(\mathbf{\Lambda}^{-1})}{\mathrm{Tr}(\mathbf{\Lambda}^{-1/2}\mathbf{\Delta}^{1/2})}\frac{1}{\sqrt{\lambda_{i,i}\delta_{i,i}}} - \frac{1}{\lambda_{i,i}\delta_{i,i}}, \quad (43)$$

where $\lambda_{i,i}$ and $\delta_{i,i}$ are the eigen values of the diagonal matrices $\mathbf{\Lambda}$ and $\mathbf{\Delta}$ respectively. Finally, with the knowledge of the effective channel matrix $\mathbf{H}_F$ and the knowledge of the diagonal matrices $\mathbf{\Delta}$, $\mathbf{\Lambda}$ corresponding to the eigen decomposition in (38), (39), the optimal digital precoder-combiner combination that minimizes the mean square error of the digital waveform in the receiver can be written as

$$\mathbf{F}_{BB}^{opt} = \mathbf{V}\mathbf{\Phi}\mathbf{U}^H. \quad (44)$$

$$\mathbf{W}_{BB}^{opt} = \mathbf{R}_{dd}\mathbf{F}_{BB^{opt}}^H\mathbf{H}_F^H\Big(\mathbf{H}_F\mathbf{F}_{BB}^{opt}\mathbf{R}_{dd}\mathbf{F}_{BB^{opt}}^H\mathbf{H}_F^H + \mathbf{R}_{nn}\Big)^{-1}. \quad (45)$$

Therefore, such a joint design of the optimal precoder and combiner minimizes the MSE of the digital waveform at the receiver in the high sampling domain, given channel state information and the covariance information of the waveform and noise. Now receiver-specific signal processing with respect to the proposed waveform design can be performed to separate the original information corresponding to the individual subbands.

C. THZ HYBRID MIMO SYSTEM WITH BAND-WISE PRECODING/COMBINING IN THE LOW SAMPLING DOMAIN

In this subsection, we describe the proposed hybrid architecture for MB-OFDM with beamforming in the low sampling domain. We propose a hybrid MIMO scheme that incorporates multiple low-dimensional digital precoders and combiners operating in the low-sampling domain, each associated with a subband and functioning at a lower clock speed. Digital precoding and combining are performed in the frequency domain, based on corresponding bandwise channel information and the analog RF precoder is common for all subbands. The complete transmitter architecture of the proposed scheme is given in Fig. 5.

We consider capacity as the cost function in the design of the hybrid beamformers in this scenario. The total capacity of the system can be expressed as the sum of the capacities of the individual subbands.

Thus, the objective of the optimization problem is the design of the optimal hybrid precoders at the transmitter and the optimal hybrid combiners at the receiver such that the overall capacity of the system is maximized with the total transmit power constraint.

We express the capacity R of the wideband THz MIMO system as follows

$$R = \sum_{m=1}^{M} R^m, \tag{46}$$

where R^m is the capacity of the m^{th} subband. The R^m is computed over all the effective non-zero subcarriers in the subband as follows

$$R^m = \sum_{k=1}^{K_e^m} R^m[k], \tag{47}$$

where K_e^m is the effective number of non zero subcarriers in the m^{th} subband. According to the hybrid MIMO scheme with the proposed waveform design, the effective baseband data model in the frequency domain after the analog combining for the m^{th} subband is given by

$$\mathbf{y}^m[k] = \mathbf{W}_{RF}^H \mathbf{H}_d^m[k] \mathbf{F}_{RF} \mathbf{F}_{BB}^m[k] \mathbf{b}^m[k] + \mathbf{W}_{RF}^H \mathbf{n}^m[k], \tag{48}$$

where $\mathbf{y}^m[k]$ is the frequency domain received data vector corresponding to the m^{th} subband, $\mathbf{H}_d^m[k]$ is the frequency domain channel corresponding to the m^{th} subband's effective down-sampled MIMO channel, $\mathbf{b}^m[k]$ is the frequency domain symbol vector corresponding to the m^{th} subband, $\mathbf{F}_{BB}^m[k]$ is the baseband precoder corresponding to the m^{th} subband, $\mathbf{F}_{RF}$,$\mathbf{W}_{RF}$ are the common analog precoder and combiner and $\mathbf{n}^m[k]$ is the noise vector corresponding to the m^{th} subband. Thus, the final data model in the frequency domain after the baseband digital combining at the m^{th} subband can be written as

$$\begin{aligned}\tilde{\mathbf{y}}^m[k] = {} & \mathbf{W}_{BB}^m[k]^H \mathbf{W}_{RF}^H \mathbf{H}_d^m[k] \mathbf{F}_{RF} \mathbf{F}_{BB}^m[k] \mathbf{b}^m[k] \\ & + \mathbf{W}_{BB}^m[k]^H \mathbf{W}_{RF}^H \mathbf{n}^m[k],\end{aligned} \tag{49}$$

where $\mathbf{W}_{BB}^m[k]$ is the digital baseband combiner corresponding to the m^{th} subband. Then, the spectral efficiency per subcarrier for the m^{th} subband $R^m[k]$ can be expressed as follows

$$R^m[k] = \log_2 \left| \mathbf{I}_{N_r} + \frac{1}{\sigma^2} \mathbf{C}^m[k] \mathbf{H}_d^m[k] \mathbf{F}^m[k] \mathbf{F}^m[k]^H \mathbf{H}_d^m[k]^H \right|, \tag{50}$$

where $\mathbf{C}^m[k] = \mathbf{W}^m[k](\mathbf{W}^m[k]^H \mathbf{W}^m[k])^{-1} \mathbf{W}^m[k]^H$, $\mathbf{F}^m[k] = \mathbf{F}_{RF} \mathbf{F}_{BB}^m[k]$ and $\mathbf{W}^m[k] = \mathbf{W}_{RF} \mathbf{W}_{BB}^m[k]$. Thus the optimization problem for ultra-wideband THz hybrid MIMO system can be formulated as

$$\begin{aligned}\underset{\mathbf{F}_{RF}, \mathbf{W}_{RF}, \mathbf{F}_{BB}^m[k], \mathbf{W}_{BB}^m[k]_{m\in[M],k\in[K]}}{\arg} \quad & \max \sum_{m=1}^{M} R^m \\ \text{s.t.} \quad & 1. \sum_{m=1}^{M} \sum_{k=1}^{k=K} \mathrm{Tr}\left(\mathbf{F}_{RF} \mathbf{F}_{BB}^m[k] \mathbf{F}_{BB}^m[k]^H \mathbf{F}_{RF}^H \right) \leq P_{tot} \\ & 2. \quad |\mathbf{F}_{RF}(i,j)| = 1, \forall (i,j) \\ & 3. \quad |\mathbf{W}_{RF}(i,j)| = 1, \forall (i,j),\end{aligned} \tag{51}$$

where P_{tot} is the total transmit power constraint. The total power constraint can be expressed as $P_{tot} = \sum_{m=1}^{M} P_m$, where $P_m = \sum_{k=1}^{K_e^m} ||\mathbf{F}_{RF} \mathbf{F}_{BB}^m[k]||^2$ is the power allotted to the m^{th} subband. As the joint optimization of all parameters is computationally complex, we adopt a sub-optimal approach. First, the hybrid precoders at the transmitter are designed by assuming optimal combiners at the receiver. Then once the optimal transmit hybrid precoders are available, that information is used to further optimize the hybrid combiners at the receiver as outlined in [10], [12], [13]. Since this joint optimization problem is difficult to solve with the total transmit power constraint, a band-wise power constraint is assumed in each subband. Based on that, we do a band-wise optimization to find out the optimal baseband digital precoders and combiners corresponding to each of the subbands.

1) SUB-OPTIMAL HYBRID PRECODERS DESIGN

The hybrid precoders at the transmitter include the multiple baseband digital precoders corresponding to the individual subbands and the analog precoder, which is common to all the subbands. Thus, the transmitter hybrid precoding problem can be written as

$$\begin{aligned}\underset{\{\mathbf{F}_{RF}, \mathbf{F}_{BB}^m[k],\}_{m\in[M],k\in[K_e^m]}}{\arg} \quad & \max \sum_{m=1}^{M} R^m \\ \text{s.t.} \quad & 1. \sum_{m=1}^{M} \sum_{k=1}^{k=K_e^m} Tr\left(\mathbf{F}_{RF} \mathbf{F}_{BB}^m[k] \mathbf{F}_{BB}^m[k]^H \mathbf{F}_{RF}^H \right) \leq P_{tot}, \\ & 2. \ |\mathbf{F}_{RF}(i,j)| = 1, \forall (i,j),\end{aligned} \tag{52}$$

where $P_{tot} = \sum_{m=1}^{M} P_m$, is the total transmit power constraint. This problem can be solved by first fixing an analog beamformer $\mathbf{F}_{RF}$ which is common for all the subbands, and then designing the optimal digital precoders $\mathbf{F}_{BB}^m[k]$ of each band in such a way that the overall capacity in the subband is maximized with the corresponding band-wise power constraint. To further simplify the problem, we assume an equal power division among subbands and do a band-wise optimization considering an average per subcarrier power constraint in each subband to obtain the optimal baseband precoders corresponding to each of the subbands. Thus, the transmitter digital baseband precoder design problem for the m^{th} subband can be written as

$$\begin{aligned}\underset{\mathbf{F}_{BB}^m[k]}{\arg} \quad & \max \sum_{k=1}^{K_e^m} R^m[k] \\ \text{s.t.} \quad & Tr\left(\mathbf{F}_{RF} \mathbf{F}_{BB}^m[k] \mathbf{F}_{BB}^m[k]^H \mathbf{F}_{RF}^H \right) \leq P_{av}^m\end{aligned} \tag{53}$$

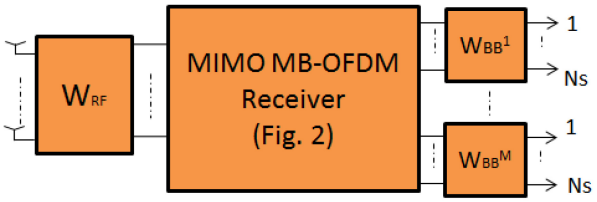

FIGURE 6. Receiver architecture for ultra-wideband THz MIMO with band-wise precoders/combiners.

where P_{av}^m is the average per subcarrier power constraint in the m^{th} band and $R^m[k]$, the achievable rate of subcarrier k in the m^{th} subband, is given by

$$R^m[k] = \log_2\left|\mathbf{I}_{N_r} + \frac{1}{\sigma^2}\mathbf{H}_d^m[k]\mathbf{F}^m[k]\mathbf{F}^m[k]^H\mathbf{H}_d^m[k]^H\right|. \quad (54)$$

Due to the coupling between the RF and baseband precoders in the power constraint, the optimal baseband precoders are expressed as a function of RF precoders as described in [13], [14]. Even when the RF precoder is fixed, the effective channel at the baseband is different in different subbands due to the unique frequency-dependent nature of the wideband THz channel. Therefore, once the analog precoder is fixed, the effective channel corresponding to the m^{th} subband can be written as $\mathbf{H}_{ef}^m[k] = \mathbf{H}_d^m[k]\mathbf{F}_{RF}$. So, the optimal digital precoder corresponding to the m^{th} subband can be found by solving

$$\begin{aligned}\underset{\mathbf{F}_{BB}^m[k]}{\arg\max}\ & \log_2\left|\mathbf{I}_{N_r} + \frac{1}{\sigma^2}\mathbf{H}_{ef}^m[k]\mathbf{F}_{BB}^m[k]\mathbf{F}_{BB}^m[k]^H\mathbf{H}_{ef}^m[k]^H\right| \\ \text{s.t.}\ & Tr\left(\mathbf{Q}\mathbf{F}_{BB}^m[k]\mathbf{F}_{BB}^m[k]^H\right) \le P_{av}^m, \end{aligned} \quad (55)$$

where $\mathbf{Q} = \mathbf{F}_{RF}^H\mathbf{F}_{RF}$. Thus, the digital baseband precoding matrix for the m^{th} subband is given by the closed-form solution

$$\mathbf{F}_{BB}^m[k] = \mathbf{Q}^{-1/2}\mathbf{V}_e^m[k]\mathbf{\Gamma}_e^m[k], \quad (56)$$

where $\mathbf{V}_e^m[k]$ is the set of right singular vectors corresponding to the largest N_s singular values of $\mathbf{H}_{ef}^m[k]\mathbf{Q}^{-1/2}$ and $\mathbf{\Gamma}_e^m[k]$ is the diagonal matrix representing the water-filling power solution. More details are given in Appendix. Hence, the optimal digital precoders for the different subbands are dependent only on the band-wise channel information $\mathbf{H}_d^m[k]$ and the analog precoding matrix $\mathbf{F}_{RF}$. That is, given the power constraint and the band-wise channel information, we obtain the optimal baseband precoders that maximize the spectral efficiency in the corresponding subbands. For simplicity, we fix the RF precoder based on the standard mean channel matrix (MCM) and mean channel covariance matrix (MCCM) based analog beamforming algorithms [19], [36] by utilizing the channel information of subcarriers in all the subbands.

TABLE 1. List of parameters.

Name of parameter	Value (Default)
RF	300 GHz
Input Bandwidth	30 GHz
No of Subbands	5 (Default)
Subband Width	6 GHz
Channel model	Filter bank model
No of Dominant Paths	5
Array type	ULA
Array architecture	Fully connected
Noise Power	As per the SNR
Modulation	QPSK
FFT Size	512
No. of Tx Antennas	20
No. of Rx Antennas	20

2) SUB-OPTIMAL HYBRID COMBINERS DESIGN

The hybrid combiners at the receiver include the multiple band-wise digital baseband combiners and the analog combiner, common to all the subbands. The hybrid combiner design is carried out using the already obtained hybrid precoders. In this work, we fix the RF combiner by setting the columns as the array response vectors corresponding to the propagation paths at the receiver. After that, for the already fixed RF combiner, we find the optimal baseband combiners in each subband. The optimal digital combiner for the m^{th} subband corresponding to the k^{th} subcarrier for a given analog combiner is denoted as $\mathbf{W}_{BB}^m[k]$ and is given by the standard minimum mean square error (MMSE) solution as

$$\mathbf{W}_{BB}^m[k] = \mathbf{J}^m[k]^{-1}\mathbf{W}_{RF}^H\mathbf{H}_d^m[k]\mathbf{F}^m[k], \quad (57)$$

where

$$\mathbf{J}^m[k] = \mathbf{W}_{RF}^H\mathbf{H}_d^m[k]\mathbf{F}^m[k]\mathbf{F}^m[k]^H\mathbf{W}_{RF} + \sigma^2\mathbf{W}_{RF}^H\mathbf{W}_{RF} \quad (58)$$

and $\mathbf{F}^m[k] = \mathbf{F}_{RF}\mathbf{F}_{BB}^m[k]$ is the effective precoder corresponding to the m^{th} subband. The overall algorithm for the precoder and combiner design is given in Algorithm 1.

V. RESULTS AND DISCUSSION

In this section, we present the numerical results of our proposed THz hybrid MIMO schemes. Our evaluation focuses on the bit error rate (BER) and spectral efficiencies of the schemes which we assess under different system parameter assumptions to verify the effectiveness of our proposed schemes. Given the lack of availability of real THz measurements and the frequency dependency of the baseband channel coefficients, we make different subband width assumptions and parameters for the purposes of simulation. Beam squint effect is not considered for simplicity. We assume an indoor wideband THz wireless system with perfect channel information, a fully connected architecture, and a ULA for beamforming at both the transmitter and receiver. The various simulation parameters are shown in Table 1.

Algorithm 1 Band-Wise Precoder/Combiner Design for MIMO MB-OFDM THz System

Given $\mathbf{H}^m[k], k = 1, 2, \ldots K, m = 1, 2, \ldots M$
Initialize Mean channel matrix $\bar{\mathbf{H}} = \mathbf{0}_{N_r \times N_t}$, Mean channel covariance matrix $\mathbf{H}_c = \mathbf{0}_{N_t \times N_t}$
if MCM **then**
  for $m = 1 : M$ **do**
    for $k = 1 : K$ **do**
      $\bar{\mathbf{H}} = \bar{\mathbf{H}} + \mathbf{H}^m[k]$
    end for
  end for
  Set $\bar{\mathbf{H}} = \frac{\bar{\mathbf{H}}}{MK}$
  $\bar{\mathbf{H}} = \bar{\mathbf{U}}\bar{\Sigma}\bar{\mathbf{V}}^H$
  Set $\mathbf{F}_{RF} = \bar{\mathbf{V}}(:, 1 : N_{RF})$
else if MCCM
  for $m = 1 : M$ **do**
    for $k = 1 : K$ **do**
      $\mathbf{H}_c = \mathbf{H}_c + \mathbf{H}^m[k]^H\mathbf{H}^m[k]$
    end for
  end for
  Set $\mathbf{H}_c = \frac{\mathbf{H}_c}{MK}$
  $\mathbf{H}_c = \mathbf{U}_c\Sigma_c\mathbf{V}_c$
  Set $\mathbf{F}_{RF} = \mathbf{V}_c(:, 1 : N_{RF})$
end if
for $m = 1 : M$ **do**
  for $k = 1 : K$ **do**
    $\mathbf{F}^m_{BB}[k] = (\mathbf{F}^H_{RF}\mathbf{F}_{RF})^{-1/2}\mathbf{V}^m_e[k]\mathbf{\Gamma}^m_e[k]$
  end for
end for
Set $\mathbf{W}_{RF}$ as ARVs of channel paths at Rx
for $m = 1 : M$ **do**
  for $k = 1 : K$ **do**
    $\mathbf{W}^m_{BB}[k] = \mathbf{J}^m[k]^{-1}\mathbf{W}^H_{RF}\mathbf{H}^m[k]\mathbf{F}^m[k]$
  end for
end for

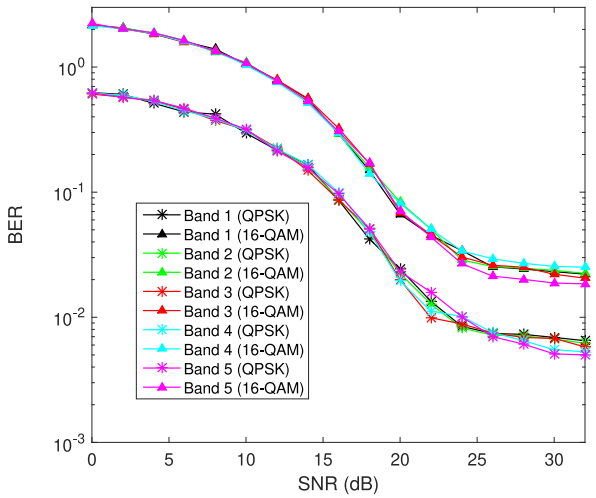

FIGURE 7. Bandwise BER performance with single precoder/combiner in the high sampling domain with $N_z = 5$, $N_t = 20$, $N_r = 20$, and bandwidth of 30 GHz split into five subbands with FFT size $K = 512$.

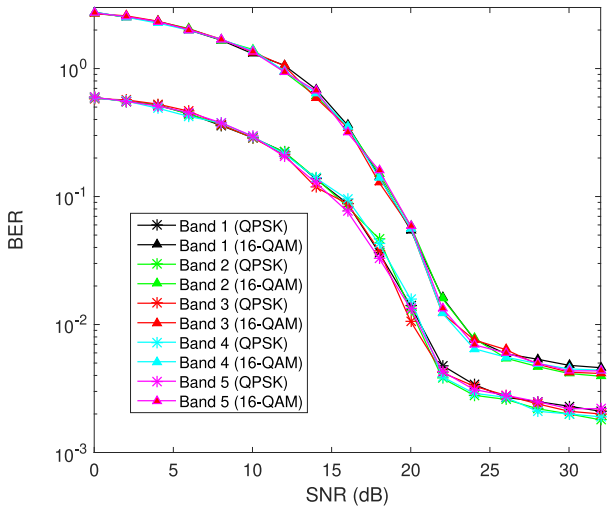

FIGURE 8. Bandwise BER performance with single precoder/combiner in the high sampling domain with $N_z = 10$, $N_t = 20$, $N_r = 20$ and bandwidth of 30 GHz split into five subbands with FFT size $K = 512$.

First, we show the BER performance of the hybrid MIMO system with the single precoder and combiner in the high sampling domain. The band-wise BER performance of the system is analyzed for different values of the zero subcarriers (N_z). In this setup, we use the number of transmit antennas $N_t = 20$, the number of receive antennas $N_r = 20$, and the number of spatial streams $N_s = 2$. Here we set the analog precoder $\mathbf{F}_{RF}$ and the analog combiner $\mathbf{W}_{RF}$ as the array response vectors corresponding to the actual angles of propagation paths at the transmitter and receiver [10], [34]. The FFT size in each subband is $K = 512$ with a total bandwidth of 30 GHz subdivided into five subbands with a subband width of 6 GHz each. The corresponding bandwise BER performance is given in Fig. 7, Fig. 8 and Fig. 9 for the number of zero subcarriers $N_z = 5$, $N_z = 10$ and $N_z = 20$ respectively.

For lower number of zero subcarriers N_z, the different subbands exhibit similar BER performance in the lower SNR range. Nonetheless, as the SNR increases, each subband's BER performance starts to degrade due to interference from adjacent subbands. As the number of zero subcarriers increases from $N_z = 5$ to $N_z = 20$, we observe a corresponding improvement in the BER performance. This is attributed to the increased guard band, which provides better protection against interference from neighboring subbands. To gain further insight, we plot the average BER of the system with different values of N_z. We examine two scenarios where the number of zero subcarriers is varied. In the first scenario, we divided the total bandwidth into five subbands with a subband width of 6 GHz each and used an FFT size of $K = 256$. In the second scenario, we reduced the number of subbands to three and used an FFT size of $K = 512$. Our results, shown in Fig. 10 for the $M = 5$ case and Fig. 11 for the $M = 3$ case, demonstrate a flattening of the BER

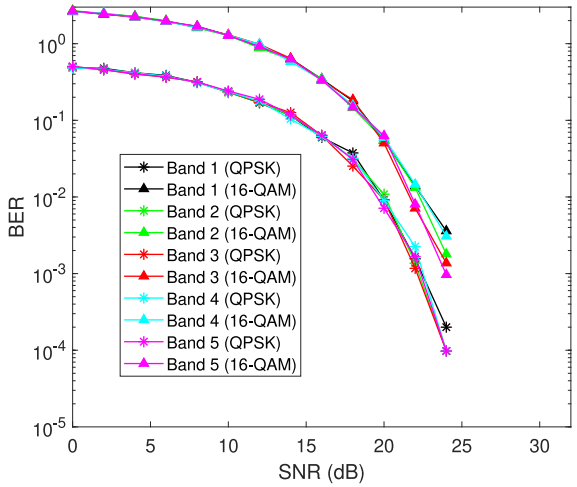

FIGURE 9. Bandwise BER performance with single precoder/combiner in the high sampling domain with $N_z = 20$, $N_t = 20$, $N_r = 20$, and bandwidth of 30 GHz split into five subbands with FFT size $K = 512$.

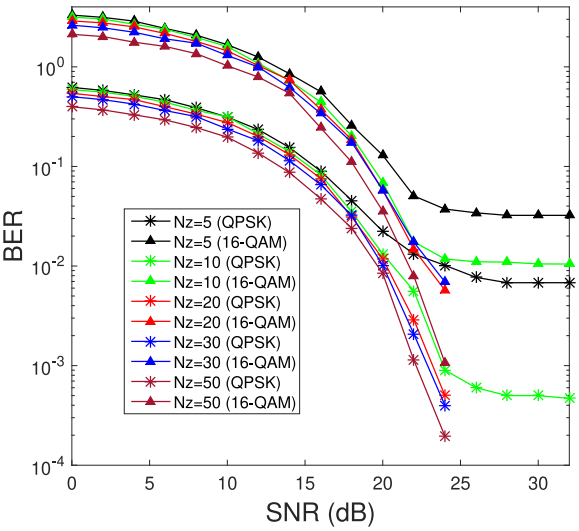

FIGURE 10. BER performance with single precoder/combiner in the high sampling domain for the different number of zero subcarriers with $N_t = 20$, $N_r = 20$, bandwidth of 30 GHz split into five subbands with FFT size $K = 256$.

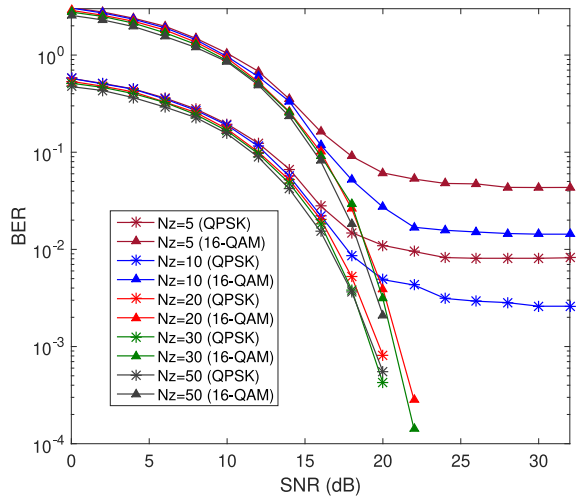

FIGURE 11. BER performance with single precoder/combiner in the high sampling domain for the different number of zero subcarriers with $N_t = 20$, $N_r = 20$, bandwidth of 30 GHz split into three subbands with FFT size $K = 512$.

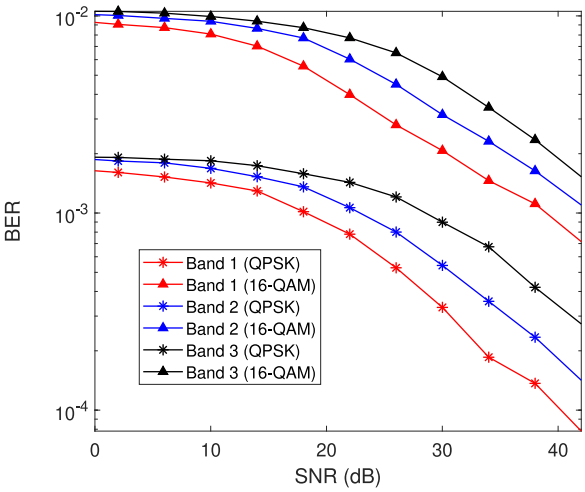

FIGURE 12. Bandwise BER performance with bandwise precoders/combiners with MCCM analog precoder; $N_t = 20$, $N_r = 20$, $N_z = 20$, and bandwidth of 30 GHz split in 3 subbands.

vs. SNR curve as N_z decreases. This phenomenon occurs because as N_z decreases, the front-end filters in the MB-OFDM system have less sharp transitions from passband to stopband, leading to increased inter-subband interference. This interference limits the ability of the system to improve its BER beyond a certain SNR threshold. However, as N_z increases, this effect becomes negligible.

Next, the performance of the hybrid MIMO system using bandwise precoders and combiners is analyzed. Specifically, the BER performance and average spectral efficiency are evaluated while keeping the common RF precoder fixed using the standard MCM and MCCM-based analog beamforming algorithms [19], [36] with channel information from all subcarriers. The system is evaluated with the same parameter set as defined in Table-1 with $M = 3$ subbands. The BER of individual subbands is plotted in Fig. 12, indicating that the hybrid MIMO system with bandwise precoding in the low sampling domain exhibits varying BER across different subbands. Specifically, the subband situated at the higher end of the RF band performs worse compared to the other subbands. This could be attributed to the lower power in the precoder for that particular subband and its position within the higher side of the RF spectrum.

The overall effective BER of the hybrid MIMO system is computed as the average of all the bandwise BER and is plotted in Fig. 13 for the same parameter settings. Different analog precoders based on MCM, MCCM algorithms, and array response vectors of channel paths are considered, and it is observed that the MCCM-based analog precoding provides better overall BER performance compared to the other precoders. We have also plotted the BER performance with existing MIMO-OFDM based THz system [16] and

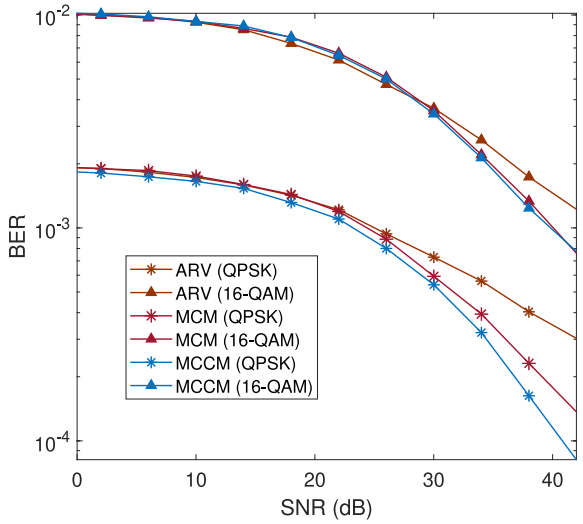

FIGURE 13. BER performance with bandwise precoding/combining in low sampling domain with different analog precoders; $N_t = 20$, $N_r = 20$, $N_z = 20$, bandwidth of 30 GHz with $M = 3$.

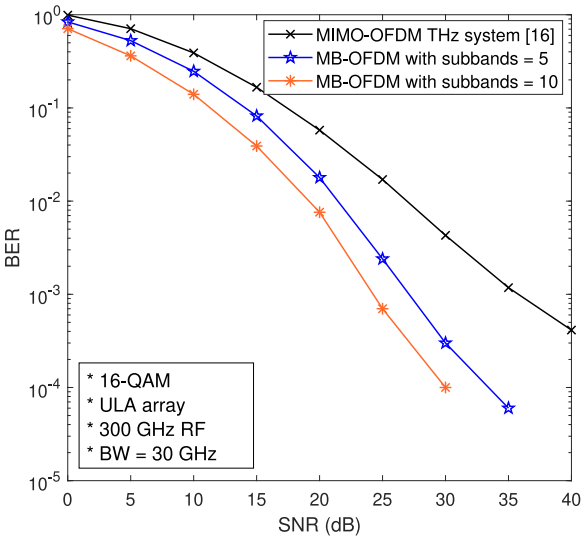

FIGURE 14. BER performance with bandwise precoding/combining in low sampling domain with different subbands and standard OFDM (M = 1). precoders; $N_t = 20$, $N_r = 20$, $N_z = 20$, bandwidth of 30 GHz.

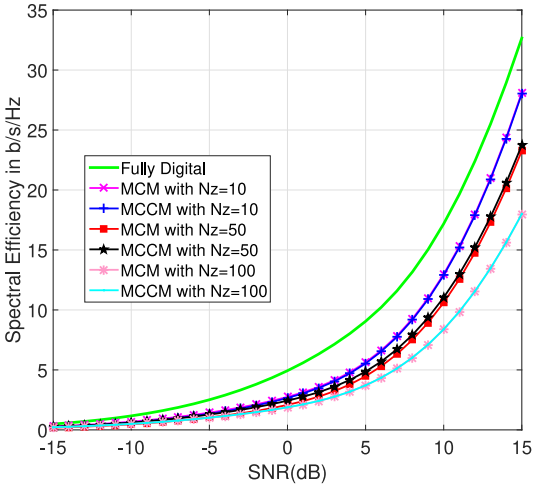

FIGURE 15. The comparison of average spectral efficiency with bandwise precoders/combiners for different N_z with $N_t = 20$, $N_r = 20$, $N_s = 2$, $M = 3$ and $K = 512$.

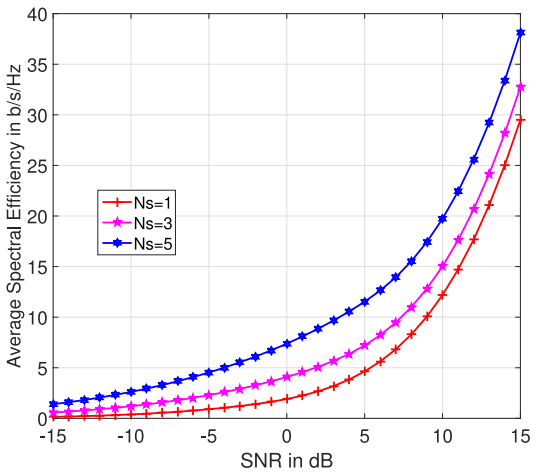

FIGURE 16. The comparison of average spectral efficiency with bandwise precoders/combiners for different N_s with $N_t = 30$, $N_r = 30$, $M = 5$ and $K = 512$ with MCM based analog precoder.

varying the subband number in Fig. 14. We observe almost 5 dB SNR gain with respect to conventional MIMO-OFDM Thz system at around 10^{-3} BER. This is due to frequency dependency of the channel taps in wideband, which is not addressed in OFDM system. We also observe SNR gain when number of subbands (M) are increased, which establishes the superiority of the MB-OFDM system.

Next, the performance of the proposed ultra-wideband hybrid MIMO system, which uses bandwise precoding/combining is evaluated in terms of its average spectral efficiency. The system performance is presented in Fig. 15, which illustrates the average spectral efficiency for a bandwidth of 30 GHz, $N_t = 20$ transmitting antennas, $N_r = 20$ receiving antennas, $N_s = 2$ streams, and an FFT size of $K = 512$. The analysis considers the impact of different analog precoder choices and various numbers of zero subcarriers on the system's overall spectral efficiency. The results demonstrate that as the number of zero subcarriers increases, the system's spectral efficiency decreases, regardless of the analog precoder selected. This reduction occurs because more zero subcarriers eliminate interference from neighboring subbands, but it reduces the number of effective non-zero subcarriers available for data transmission in each subband. Consequently, in practical scenarios, the values of zero subcarriers should be optimally chosen based on the system's THz range of operation and the desired BER performance requirement. In Fig. 16, we compare the average spectral efficiency of the proposed scheme for different numbers of data streams, namely $N_s = 1$, $N_s = 3$, and $N_s = 5$. The system parameters are changed and set as follows: $N_t = 30$ transmitting antennas, $N_r = 30$ receiving antennas, $N_z = 30$ zero subcarriers,

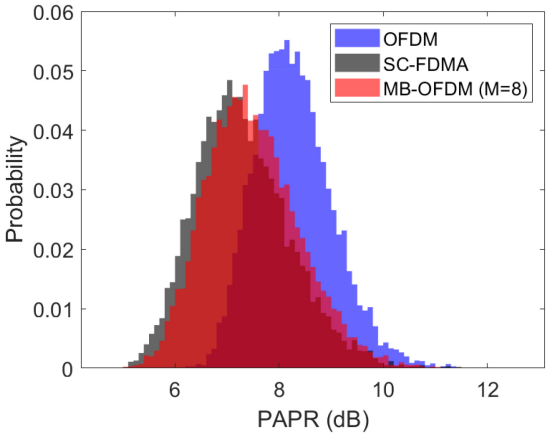

FIGURE 17. The comparison of the PAPR in terms of histograms for the proposed MB-OFDM with conventional OFDM and SC-FDMA with the total number of subcarriers fixed at 512 and the number of subbands $M = 8$ with QPSK modulation.

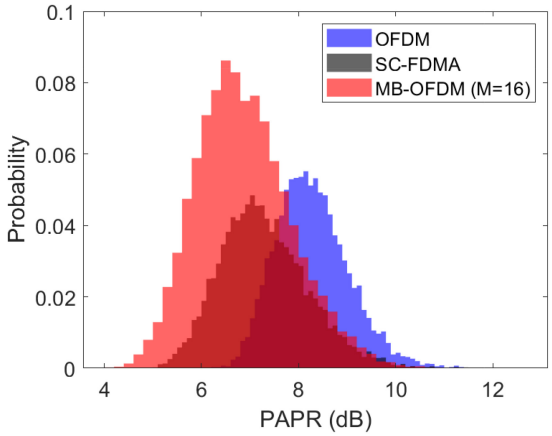

FIGURE 19. The comparison of the PAPR in terms of histograms for the proposed MB-OFDM with conventional OFDM and SC-FDMA with the total number of subcarriers fixed at 512 and the number of subbands $M = 16$ with QPSK modulation.

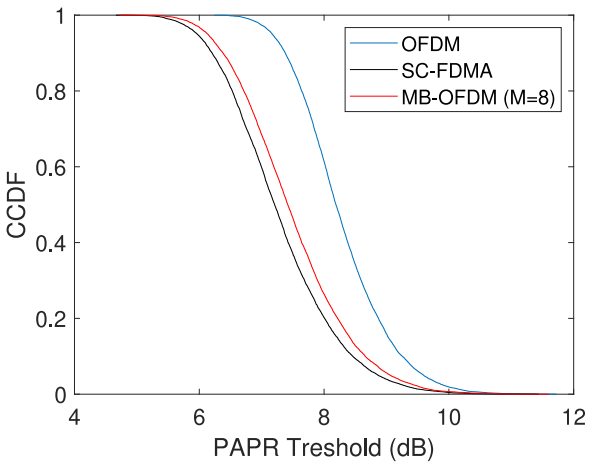

FIGURE 18. The comparison of the PAPR in terms of CCDF for the proposed MB-OFDM with conventional OFDM and SC-FDMA with the total number of subcarriers fixed at 512 and the number of subbands $M = 8$ with QPSK modulation.

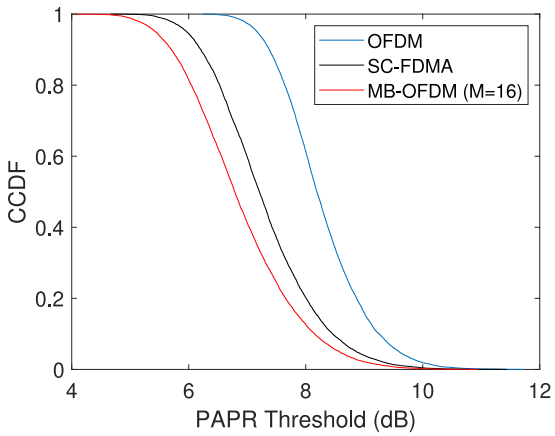

FIGURE 20. The comparison of the PAPR in terms of CCDF for the proposed MB-OFDM with conventional OFDM and SC-FDMA with the total number of subcarriers fixed at 512 and the number of subbands $M = 16$ with QPSK modulation.

an FFT size of $K = 512$, a bandwidth of 30 GHz with 5 subbands with a subband width of 6 GHz each. By effectively transmitting multiple data streams with minimal interference through sufficient zero padding, the system's average spectral efficiency performance improves with an increase in the number of spatial streams.

We now present the simulation results showing the PAPR of the baseband spatial streams using the proposed MB-OFDM waveform and compare it with conventional OFDM, and single carrier frequency division multiple access (SC-FDMA) with a pre-FFT size of 128. We employ QPSK modulation and maintain the total number of subcarriers constant at 512.To depict the PAPR distribution for each scheme, histograms averaged over numerous realizations are plotted. In Fig. 17, we compare the PAPR of conventional OFDM and SC-FDMA with that of the proposed MB-OFDM using $M = 8$. Additionally, the corresponding PAPR comparison, represented through the complementary cumulative distribution function (CCDF), is illustrated in Fig. 18. Similarly, Fig. 19 and Fig. 20 demonstrate the histogram and respective CCDF as the number of subbands is increased to $M = 16$. The results distinctly establish the superiority of MB-OFDM over conventional OFDM. The performance of SC-FDMA is slightly better than MB-OFDM in the $M = 8$ case. However, we can see a significant reduction in the PAPR for the proposed waveform when the number of subbands is increased from $M = 8$ to $M = 16$ and it shows a better performance compared to both SC-FDMA and conventional OFDM. The proposed MB-OFDM scheme significantly reduces PAPR by using the specialized baseband design for THz, which divides the wideband into smaller subbands. Although the front-end filter following upsampling in each subband can potentially increase PAPR [37], this effect is balanced by the lower number of subcarriers in each subband, reducing peak power [38]. Consequently, the likelihood of peaks occurring simultaneously across all subbands decreases, leading to an

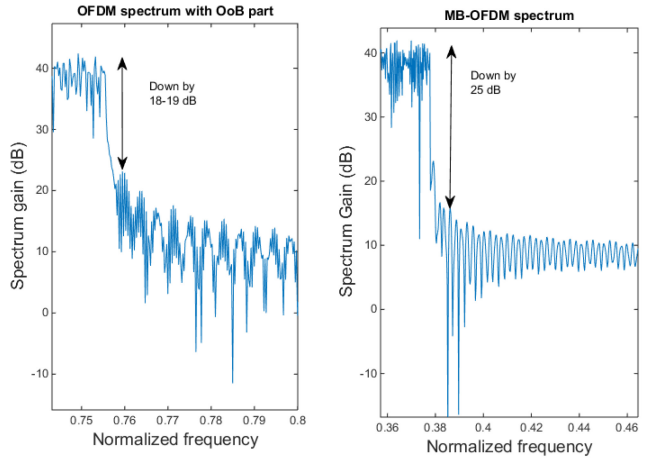

FIGURE 21. The comparison of the OoB emission for the proposed MB-OFDM (M = 2) with conventional OFDM.

overall reduction in PAPR compared to a single wideband OFDM signal [32].

Next, we evaluate the OoB emission reduction capability of MB-OFDM compared to conventional OFDM. To illustrate the OoB reduction performance, we consider an MB-OFDM system with $M = 2$ subbands. The results, depicted in Fig. 21, show a significant improvement in OoB emission reduction with the MB-OFDM architecture. Specifically, while the conventional OFDM spectrum exhibits a reduction of approximately 18 dB, the MB-OFDM system achieves a significantly higher reduction of approximately 25 dB. This enhanced performance clearly demonstrates the superior ability of the MB-OFDM-based system to mitigate OoB emissions, validating its effectiveness over traditional OFDM systems. The improvements in PAPR reduction and OoB emission control highlight the potential advantages of implementing the proposed waveform in wideband THz MIMO communication. By effectively mitigating PAPR and addressing the frequency-dependent characteristics inherent in wideband THz channels, this approach can significantly enhance the overall performance of THz systems.

VI. CONCLUSION

This work presents a novel THz-specific MIMO baseband system design that mitigates the ultra-wideband and unfavourable frequency-dependent challenges associated with the THz channel. We have proposed two hybrid MIMO architectures with the proposed THz-specific MB-OFDM waveform. The first architecture uses a single precoder and combiner in the high-sampling domain, while the second one employs multiple bandwise digital precoders/combiners operating in the low-sampling domain. Our extensive numerical simulations, with varying parameters and subband width assumptions, demonstrate the feasibility and effectiveness of the proposed schemes for communication in ultra-wideband frequency-dependent THz channels. We also show that the proposed waveform design reduces the PAPR of the system compared to the conventional OFDM.

APPENDIX

The optimal digital precoder corresponding to the m^{th} subband can be found by solving

$$\arg\max_{\mathbf{F}^m_{BB}[k]} \log_2\left|\mathbf{I}_{N_r} + \frac{1}{\sigma^2}\mathbf{H}^m_{ef}[k]\mathbf{F}^m_{BB}[k]\mathbf{F}^m_{BB}[k]^H\mathbf{H}^m_{ef}[k]^H\right|$$
$$\text{s.t. } Tr\left(\mathbf{Q}\mathbf{F}^m_{BB}[k]\mathbf{F}^m_{BB}[k]^H\right) \le P^m_{av}, \tag{59}$$

where $\mathbf{Q} = \mathbf{F}^H_{RF}\mathbf{F}_{RF}$. Here, the optimal baseband precoders cannot be directly derived from a simple SVD of the effective channel combined with the RF precoder $\mathbf{H}^m_{ef}[k] = \mathbf{H}^m_d[k]\mathbf{F}_{RF}$. This is due to the distinct power constraints that arise from the interaction between the baseband and RF precoders.

By making the change of variables $\mathbf{F}^m_{BB}[k] = \mathbf{Q}^{-1/2}\tilde{\mathbf{F}}^m_{BB}[k]$, where $\mathbf{Q} = \mathbf{F}^H_{RF}\mathbf{F}_{RF}$ and $\tilde{\mathbf{F}}^m_{BB}[k]$ is the equivalent baseband precoder, we can rewrite the optimization problem as

$$\arg\max_{\tilde{\mathbf{F}}^m_{BB}[k]} \log_2\left|\mathbf{I}_{N_r} + \frac{1}{\sigma^2}\mathbf{H}^m_{ef}[k]\mathbf{Q}^{-1/2}\tilde{\mathbf{F}}^m_{BB}[k]\tilde{\mathbf{F}}^m_{BB}[k]^H \times\mathbf{Q}^{-1/2}\mathbf{H}^m_{ef}[k]^H\right|$$
$$\text{s.t. } Tr\left(\tilde{\mathbf{F}}^m_{BB}[k]\tilde{\mathbf{F}}^m_{BB}[k]^H\right) \le P^m_{av} \tag{60}$$

The equivalent optimization problem is now transformed into a MIMO precoder design problem with the objective of maximizing mutual information with the effective channel matrix $\mathbf{H}^m_{ef}[k]\mathbf{Q}^{-1/2}$. Consequently, the optimal equivalent baseband precoder can be expressed as follows

$$\tilde{\mathbf{F}}^m_{BB}[k] = \mathbf{V}^m_e[k]\mathbf{\Gamma}^m_e[k] \tag{61}$$

where $\mathbf{V}^m_e[k]$ is the set of right singular vectors corresponding to the largest N_s singular values of the effective channel matrix $\mathbf{H}^m_{ef}[k]\mathbf{Q}^{-1/2}$ and $\mathbf{\Gamma}^m_e[k]$ is the diagonal matrix representing the water-filling power solution. Thus, the digital baseband precoding matrix for the m^{th} subband is given by the closed-form solution

$$\mathbf{F}^m_{BB}[k] = \mathbf{Q}^{-1/2}\mathbf{V}^m_e[k]\mathbf{\Gamma}^m_e[k], \tag{62}$$

REFERENCES

[1] I. F. Akyildiz, J. M. Jornet, and C. Han, "Terahertz band: Next frontier for wireless communications," *Phys. Commun.*, vol. 12, pp. 16–32, Sep. 2014. [Online]. Available: http://dx.doi.org/10.1016/j.phycom.2014.01.006

[2] I. F. Akyildiz, J. M. Jornet, and C. Han, "TeraNets: Ultra-broadband communication networks in the terahertz band," *IEEE Wireless Commun.*, vol. 21, no. 4, pp. 130–135, Aug. 2014.

[3] H. Sarieddeen, M.-S. Alouini, and T. Y. Al-Naffouri, "An overview of signal processing techniques for terahertz communications," *Proc. IEEE*, vol. 109, no. 10, pp. 1628–1665, Oct. 2021.

[4] J. M. Jornet and I. F. Akyildiz, "Channel modeling and capacity analysis for electromagnetic wireless nanonetworks in the Terahertz band," *IEEE Trans. Wireless Commun.*, vol. 10, no. 10, pp. 3211–3221, Oct. 2011.

[5] C. Han, A. O. Bicen, and I. F. Akyildiz, "Multi-ray channel modeling and wideband characterization for wireless communications in the Terahertz band," *IEEE Trans. Wireless Commun.*, vol. 14, no. 5, pp. 2402–2412, May 2015.

[6] R. Piesiewicz, C. Jansen, D. Mittleman, T. Kleine-Ostmann, M. Koch, and T. Kurner, "Scattering analysis for the modeling of THz communication systems," *IEEE Trans. Antennas Propag.*, vol. 55, no. 11, pp. 3002–3009, Nov. 2007.
[7] F. Sheikh et al., "Scattering and roughness analysis of indoor materials at frequencies from 750 GHz to 1.1 THz," *IEEE Trans. Antennas Propag.*, vol. 69, no. 11, pp. 7820–7829, Nov. 2021.
[8] C. L. Vernold and J. E. Harvey, "Modified Beckmann-Kirchoff scattering theory for nonparaxial angles," in *Proc. Int. Symp. Opt. Sci., Eng., Instrument.*, 1998, pp. 51–56. [Online]. Available: https://doi.org/10.1117/12.328477
[9] M. Inomata et al., "Terahertz propagation characteristics for 6G mobile communication systems," in *Proc. 15th Eur. Conf. Antennas Propagat. (EuCAP)*, 2021, pp. 1–5.
[10] O. E. Ayach, S. Rajagopal, S. Abu-Surra, Z. Pi, and R. W. Heath, "Spatially sparse precoding in millimeter wave MIMO systems," *IEEE Trans. Wireless Commun.*, vol. 13, no. 3, pp. 1499–1513, Mar. 2014.
[11] A. Alkhateeb and R. W. Heath, "Frequency selective hybrid precoding for limited feedback millimeter wave systems," *IEEE Trans. Commun.*, vol. 64, no. 5, pp. 1801–1818, May 2016.
[12] F. Sohrabi and W. Yu, "Hybrid digital and analog beamforming design for large-scale antenna arrays," *IEEE J. Sel. Topics Signal Process.*, vol. 10, no. 3, pp. 501–513, Apr. 2016.
[13] F. Sohrabi and W. Yu, "Hybrid analog and digital beamforming for mmWave OFDM large-scale antenna arrays," *IEEE J. Sel. Areas Commun.*, vol. 35, no. 7, pp. 1432–1443, Jul. 2017.
[14] S. Park, A. Alkhateeb, and R. W. Heath, "Dynamic subarrays for hybrid precoding in wideband mmWave MIMO systems," *IEEE Trans. Wireless Commun.*, vol. 16, no. 5, pp. 2907–2920, May 2017.
[15] H. Yuan, N. Yang, K. Yang, C. Han, and J. An, "Hybrid beamforming for MIMO-OFDM Terahertz wireless systems over frequency selective channels," in *Proc. IEEE Glob. Commun. Conf. (GLOBECOM)*, 2018, pp. 1–6.
[16] H. Yuan, N. Yang, K. Yang, C. Han, and J. An, "Hybrid beamforming for terahertz multi-carrier systems over frequency selective fading," *IEEE Trans. Commun.*, vol. 68, no. 10, pp. 6186–6199, Oct. 2020.
[17] R. Zhang, W. Hao, G. Sun, and S. Yang, "Hybrid precoding design for wideband THz massive MIMO-OFDM systems with beam squint," *IEEE Syst. J.*, vol. 15, no. 3, pp. 3925–3928, Sep. 2021.
[18] L. Yan, C. Han, and J. Yuan, "Energy-efficient dynamic-subarray with fixed true-time-delay design for Terahertz wideband hybrid beamforming," *IEEE J. Sel. Areas Commun.*, vol. 40, no. 10, pp. 2840–2854, Oct. 2022.
[19] Y. Wu, G. Song, H. Liu, L. Xiao, and T. Jiang, "3-D hybrid beamforming for terahertz broadband communication system with beam squint," *IEEE Trans. Broadcast.*, vol. 69, no. 1, pp. 264–275, Mar. 2023.
[20] P. Maity, S. Srivastava, S. Khatri, and A. K. Jagannatham, "Dictionary-learning (DL)-based sparse CSI estimation in multiuser Terahertz (THz) hybrid MIMO systems under hardware impairments and beam-squint effect," *IEEE Access*, vol. 10, pp. 113699–113714, 2022.
[21] S. Srivastava, A. Tripathi, N. Varshney, A. K. Jagannatham, and L. Hanzo, "Hybrid transceiver design for tera-hertz MIMO systems relying on Bayesian learning aided sparse channel estimation," *IEEE Trans. Wireless Commun.*, vol. 22, no. 4, pp. 2231–2245, Apr. 2023.
[22] J. Gao, C. Zhong, G. Ye Li, J. B. Soriaga, and A. Behboodi, "Spatially sparse precoding in wideband hybrid terahertz massive MIMO systems," *IEEE Trans. Wireless Commun.*, vol. 23, no. 3, pp. 1871–1885, Mar. 2024.
[23] T. Mao, J. Chen, Q. Wang, C. Han, Z. Wang, and G. K. Karagiannidis, "Waveform design for joint sensing and communications in millimeter-wave and low terahertz bands," *IEEE Trans. Commun.*, vol. 70, no. 10, pp. 7023–7039, Oct. 2022.
[24] T. Mao and Z. Wang, "Terahertz wireless communications with flexible index modulation aided pilot design," *IEEE J. Sel. Areas Commun.*, vol. 39, no. 6, pp. 1651–1662, Jun. 2021.
[25] J. Balakrishnan, A. Batra, and A. Dabak, "A multi-band OFDM system for UWB communication," in *Proc. IEEE Conf. Ultra Wideband Syst. Technol.*, 2003, pp. 354–358.
[26] Q. H. Abbasi, A. Alomainy, and Y. Hao, "Characterization of MB-OFDM-based ultrawideband systems for body-centric wireless communications," *IEEE Antennas Wireless Propag. Lett.*, vol. 10, pp. 1401–1404, 2011.
[27] J. Liu, G. Sun, and W.-P. Lin, "Bidirectional 60 GHz MB-OFDM wireless communication system," in *Proc. Wireless Telecommun. Symp.*, 2012, pp. 1–4.
[28] R. Zakaria and D. Le Ruyet, "A novel filter-bank multicarrier scheme to mitigate the intrinsic interference: Application to MIMO systems," *IEEE Trans. Wireless Commun.*, vol. 11, no. 3, pp. 1112–1123, Mar. 2012.
[29] R. Zakaria and D. Le Ruyet, "Theoretical analysis of the power spectral density for FFT-FBMC signals," *IEEE Commun. Lett.*, vol. 20, no. 9, pp. 1748–1751, Sep. 2016.
[30] R. Gerzaguet, D. Demmer, J.-B. Doré, and D. Ktiénas, "Block-filtered OFDM: A new promising waveform for multi-service scenarios," in *Proc. IEEE Int. Conf. Commun. (ICC)*, 2017, pp. 1–6.
[31] D. Demmer, R. Zakaria, R. Gerzaguet, J.-B. Doré, and D. Le Ruyet, "Study of OFDM precoded filter-bank waveforms," *IEEE Trans. Wireless Commun.*, vol. 18, no. 6, pp. 2889–2902, Jun. 2019.
[32] T. D. Dheerajlal, A. Madhusree, and A. K. Dutta, "An MB-OFDM based wideband THz communication system with impairment aware precoder and squint effect mitigation," *IEEE Access*, vol. 12, pp. 18122–18146, 2024.
[33] D. J. Costello, "Fundamentals of wireless communication (Tse, D. and Viswanath, P.) [book review]," *IEEE Trans. Inf. Theory*, vol. 55, no. 2, pp. 919–920, Feb. 2009. [Online]. Available: http://dblp.uni-trier.de/db/journals/tit/tit55.html# TseV09
[34] X. Gao, L. Dai, Y. Zhang, T. Xie, X. Dai, and Z. Wang, "Fast channel tracking for terahertz beamspace massive MIMO systems," *IEEE Trans. Veh. Technol.*, vol. 66, no. 7, pp. 5689–5696, Jul. 2017.
[35] A. Scaglione, G. B. Giannakis, and S. Barbarossa, "Redundant filterbank precoders and equalizers. i. unification and optimal designs," *IEEE Trans. Signal Process.*, vol. 47, no. 7, pp. 1988–2006, Jul. 1999.
[36] Y. Chen, Y. Xiong, D. Chen, T. Jiang, S. X. Ng, and L. Hanzo, "Hybrid precoding for wideband millimeter wave MIMO systems in the face of beam squint," *IEEE Trans. Wireless Commun.*, vol. 20, no. 3, pp. 1847–1860, Mar. 2021.
[37] S.-K. Deng and M.-C. Lin, "Recursive clipping and filtering with bounded distortion for PAPR reduction," *IEEE Trans. Commun.*, vol. 55, no. 1, pp. 227–230, Jan. 2007.
[38] H. Ochiai and H. Imai, "On the distribution of the peak-to-average power ratio in OFDM signals," *IEEE Trans. Commun.*, vol. 49, no. 2, pp. 282–289, Feb. 2001.

T. D. DHEERAJLAL (Graduate Student Member, IEEE) received the B.Tech. degree in electronics and communication engineering from MG University, India, and the M.Tech. from Cochin University, India. He is currently pursuing the Ph.D. degree with the G. S. Sanyal School of Telecommunications, Indian Institute of Technology, Kharagpur, India. His current research interests include wireless communication systems design, massive MIMO, OFDM, mmWave, and THz communications system design.

AMIT KUMAR DUTTA (Member, IEEE) received the B.E. degree in electronics and telecommunication engineering from IIEST (Shibpur), India, and the Ph.D. degree from the Indian Institute of Science, Bengaluru, India. He is currently an Assistant Professor with the G. S. Sanyal School of Telecommunications, Indian Institute of Technology, Kharagpur, India. He has worked with Texas Instrument Pvt. Ltd., Broadcom Ltd., Cypress Semiconductor, and NxP Ltd. for a total of almost 14 years prior to joining academics. He has an elaborate work experience in the field of signal processing, communication, and VLSI design in corporate, which included wireless system design and validation, and characterization. His current research interests include wireless communication systems design, massive MIMO, OFDM, mmWave, THz communications system design, and quantum signal processing.